

Article

Bioinspired Design and Computational Prediction of SCS Nickel Pincer Complexes for Hydrogenation of Carbon Dioxide

Xiaoyun Liu ^{1,2,3}, Bing Qiu ^{1,2,3} and Xinzheng Yang ^{1,2,3,*}

¹ State Key Laboratory for Structural Chemistry of Unstable and Stable Species, Institute of Chemistry Chinese Academy of Sciences, Beijing 100190, China; liuxiaoyun19@mails.ucas.ac.cn (X.L.); qiubing@iccas.ac.cn (B.Q.)

² School of Chemical Sciences, University of Chinese Academy of Sciences, Beijing 100049, China

³ Beijing National Laboratory for Molecular Sciences, CAS Research/Education Center for Excellence in Molecular Sciences, Beijing 100190, China

* Correspondence: xyang@iccas.ac.cn

Received: 25 February 2020; Accepted: 6 March 2020; Published: 11 March 2020

Abstract: Inspired by the structures of the active site of lactate racemase and H₂ activation mechanism of mono-iron hydrogenase, we proposed a series of sulphur–carbon–sulphur (SCS) nickel complexes and computationally predicted their potentials for catalytic hydrogenation of CO₂. Density functional theory calculations reveal a metal–ligand cooperated mechanism with the participation of a sulfur atom in the SCS pincer ligand as a proton receiver for the heterolytic cleavage of H₂. For all newly proposed complexes containing functional groups with different electron-donating and withdrawing abilities in the SCS ligand, the predicted free energy barriers for the hydrogenation of CO₂ to formic acid are in a range of 22.2–25.5 kcal/mol in water. Such a small difference in energy barriers indicates limited contributions of those functional groups to the charge density of the metal center. We further explored the catalytic mechanism of the simplest model complex for hydrogenation of formic acid to formaldehyde and obtained a total free energy barrier of 34.6 kcal/mol for the hydrogenation of CO₂ to methanol.

Keywords: lactate racemase; density functional theory; nickel; hydrogenation of CO₂

1. Introduction

Increasingly severe climate change is driving people to look for effective ways to reduce the concentration of greenhouse gases, especially carbon dioxide, in the atmosphere [1–3]. Transition metal-catalyzed CO₂ reduction has attracted increasing attention because it provides a promising way to use CO₂ as an abundant and non-toxic carbon source for the synthesis of valuable chemicals and fuels [4–6]. With the proposal of the “methanol economy” by Olah and co-workers [7–9], catalytic hydrogenation of CO₂ to methanol (CO₂ + 3H₂ → CH₃OH + H₂O) has become one of the most attractive strategies for the utilization of CO₂ as C1 building block and potential hydrogen storage material [10–14]. The above reaction usually contains three cascade catalytic cycles, CO₂ + H₂ → HCOOH, HCOOH + H₂ → CH₂O + H₂O, and CH₂O + H₂ → CH₃OH.

Although people have achieved some progresses in homogeneous catalytic hydrogenation of CO₂ with the development of base metal iron [15–17], cobalt [18], and manganese [19] catalysts in recent years, most of the experimentally reported efficient CO₂ hydrogenation catalysts contain noble metals and air- and moisture-sensitive phosphine ligands [6,20–32]. For the catalytic hydrogenation of CO₂ to methanol reaction, only a few base metal catalysts are reported so far. For example, Beller and co-workers [18] recently reported a homogeneous cobalt/triphos-based catalyst for the reduction of CO₂ at 70 bar of H₂ and 10 bar of CO₂ under 100 °C and production of methanol with turnover

numbers (TONs) up to 78. Pombeiro and co-workers [16] reported direct synthesis of methanol from CO₂ and H₂ catalyzed by an Fe(II) scorpionate complex achieved 44% yield of methanol with TONs and turnover frequencies (TOFs) up to 2387 and 167 h⁻¹, respectively, at 80 °C and 75 pressure. Bernskoetter and co-workers [17] reported an Fe(II) pincer complex for homogeneously catalytic conversion of H₂ and CO₂ to methanol with 250 psi of CO₂ and 1150 psi of H₂ at 100 °C with a TON of 590. Prakash and co-workers [19] investigated phosphorus–nitrogen–phosphorus (PNP) manganese pincer complexes for homogeneous hydrogenation of CO₂ to methanol at 80 bar and 150 °C with TONs up to 36. We can see those experimentally reported base metal catalysts relied on rigid reaction conditions and have rather low activities or methanol selectivity. The rational design of cost-effective non-noble metal catalysts for efficient conversion of H₂ and CO₂ to methanol under mild conditions (<100 °C) is still highly desirable and challenging. In addition to the above experimental studies, Yang and co-workers [33–37] computationally designed several Mn, Fe, and Co complexes as potential catalysts for the production of methanol from H₂ and CO₂. Those bio-inspired design and computational predictions indicate that metal–ligand cooperation (MLC) is essential for the formation of metal hydride complexes by heterolytic cleavage of H₂ for the reductions of CO₂ and formic acid. However, the application of nickel complexes for catalytic hydrogenation of CO₂ to methanol is still insufficiently investigated.

In our recent study, we computationally predicted a series of scorpion-like sulphur–carbon–sulphur (SCS) nickel complexes as a mimic of the active site of lactate racemase [38] for lactate racemization [39] and dehydrocoupling of ammonia–borane for transfer hydrogenation of ketones and imines [40]. However, those scorpion-like (SCS)Ni complexes are not good candidates for hydrogenation reactions because of their high barriers for H₂ activation. In Yang and Hall's computational study of monoiron hydrogenase catalysis [41], they found the heterolytic cleavage of H₂ by Fe and sulfide ligand has a rather low free energy barrier of 6.6 kcal/mol. Such results indicate that the metal center and sulfide ligand may cooperate as an intramolecular frustrated Lewis pair (FLP) for H₂ activation. Inspired by the above findings, we would like to explore the potentials of SCS nickel pincer structures for catalytic H₂ activation and (de)hydrogenation reactions.

As shown in Figure 1, we proposed an SCS nickel hydride complex (**1**) by removing the imidazole tail, replacing the substituent group coordinated to Ni with a hydride, and adding a proton to the sulfur atom (S1) in the amine side arm of the SCS ligand. **1'** is an isomer of **1** with the proton on the other sulfur atom (S2) in the SCS ligand. **A** is an anionic complex with deprotonated sulfur. Our density functional theory (DFT) calculations indicate that **A** and **1'** are 10.3 and 13.2 kcal/mol less stable than **1**, respectively, in water.

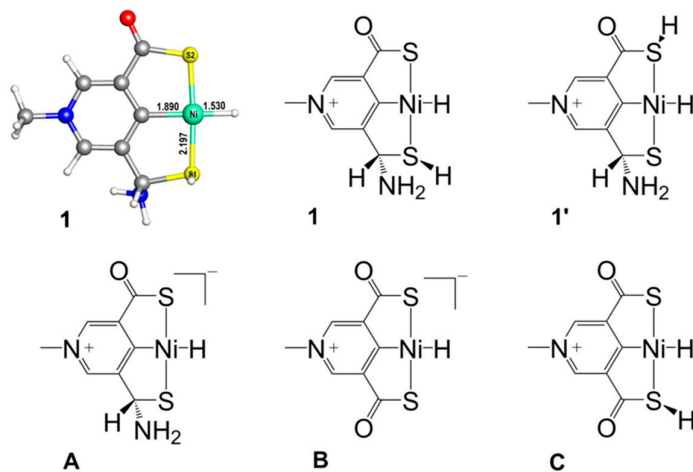


Figure 1. Proposed Ni pincer complex in this work (**1**) and its isomer with the proton on the other sulfur atom (**1'**), deprotonated structure of **1** (**A**), Ni hydride complex with Hu and co-workers' symmetric SCS pincer ligand (**B**), and **B** with a proton on sulfur (**C**).

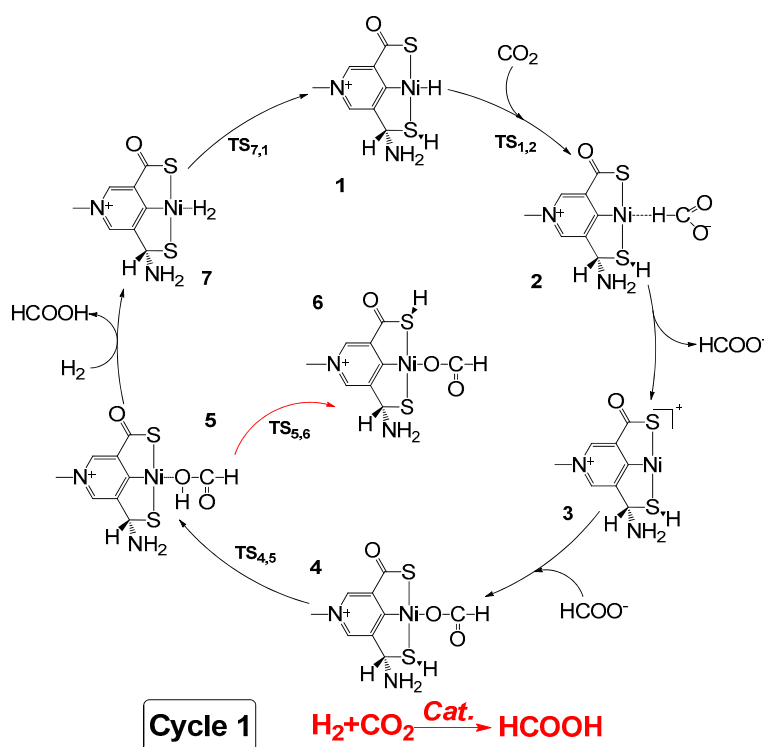
Hu and co-workers [42] recently reported three SCS nickel pincer complexes with symmetric C=O group in the arms of the pincer ligand as functional models of lactate racemase and studied their catalytic properties. Their DFT calculations suggest that the pyridinium carbon atom coordinated to Ni act as a hydride acceptor for lactate racemization, and the β -hydrogen elimination for the formation of Ni–H structure is energetically prohibitive. Figure 1 also lists a Ni hydride complex **B** with symmetric SCS pincer ligand and its protonated structure **C**, which is 7.3 kcal/mol less stable than **B** in water. Such results indicate that the C(H)(NH₂) group in the SCS ligand significantly increased the nucleophilicity of its connecting sulfur atom and is likely to facilitate H₂ activation. We also calculated the transition state for **C** to CO₂ hydride transfer and obtained a free energy barrier of 36.3 kcal/mol. Therefore, the symmetric Ni complexes with two C=O groups in the SCS ligand are unlikely to catalyze the hydrogenation of CO₂.

With the above initial analysis, we believe **1** is a relatively stable nickel hydride complex and could potentially be a catalyst or intermediate for H₂ activation and (de)hydrogenation reactions. We further investigated the detailed reaction mechanism of **1** catalyzed hydrogenation of CO₂ to formic acid, analyzed the influence of various substitutes in the SCS pincer ligand to energy barriers, and examined the catalytic activity of **1** for hydrogenation of formic acid to methanol.

2. Results and Discussion

2.1. Predicted Catalytic Cycles for the Hydrogenation of CO₂ to Formic acid

Using **1** as the starting point of the reaction, we proposed a plausible catalytic cycle (Cycle 1, Scheme 1) for the hydrogenation of CO₂ to formic acid based on DFT calculations. The corresponding relative free energies in the reaction pathway and optimized key structures in Cycle 1 are displayed in Figures 2 and 3, respectively.



Scheme 1. Predicted catalytic cycle for hydrogenation of CO₂ to formic acid (Cycle 1).

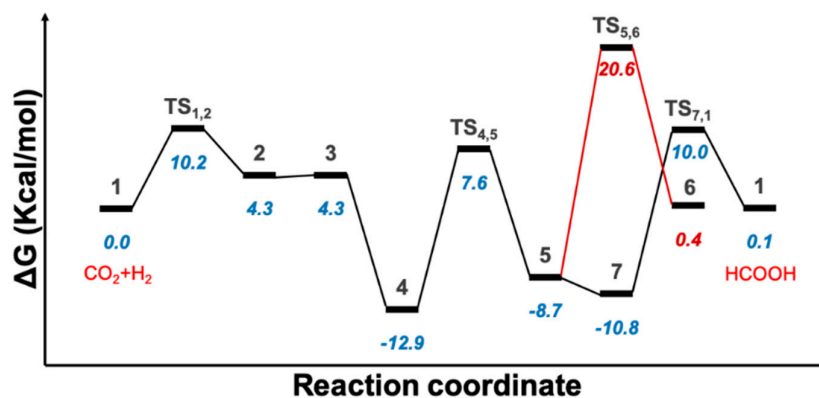


Figure 2. Free energy profile for the hydrogenation of CO₂ to formic acid catalyzed by **1**. Solvent corrected relative free energies are shown in italic with blue color.

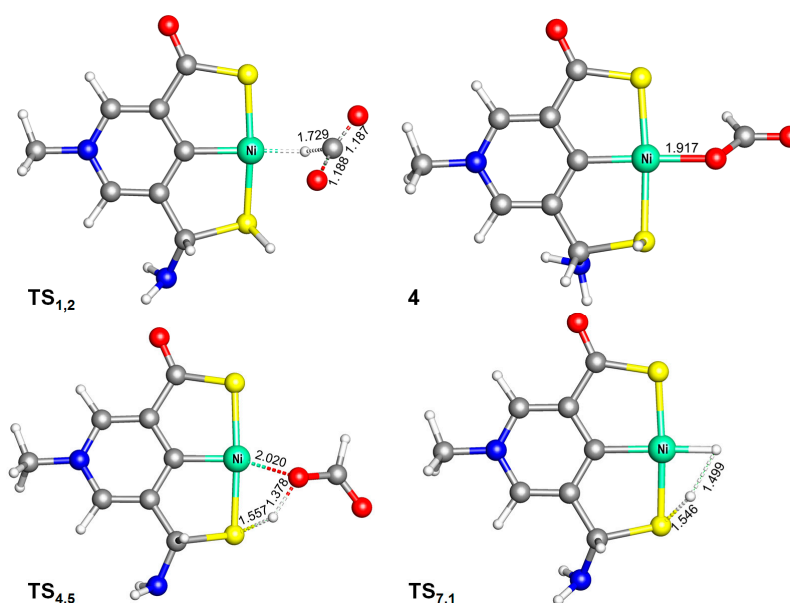


Figure 3. Optimized structures of **TS_{1,2}** (673.2i cm⁻¹), **4**, **TS_{4,5}** (1614.2i cm⁻¹), and **TS_{7,1}** (1013.6i cm⁻¹) in Cycle 1. Bond lengths are in Å.

At the beginning of the reaction, a formate anion was formed with a CO₂ molecule attacking **1** and taking the hydride on Ni through **TS_{1,2}** (Figure 3). The free energy barrier for hydride transfer from Ni to C was 10.2 kcal/mol. The formate anion in **2** could easily dissociate and come back for the formation of a much more stable intermediates **4**, which was 12.9 kcal/mol more stable than **1** because of the formation of a strong Ni–O bond (1.917 Å) in it. Then the proton on S1 transferred to the O atom bonding to Ni through **TS_{4,5}** and formed a formic acid molecule with a free energy barrier of 20.5 kcal/mol. The Ni···O distance in **5** was slightly elongated to 2.04 Å, which indicates a weaker interaction between Ni and O after the formation of the O–H bond. The HCOOH/H₂ exchange in **5** happened quickly and formed a 2.1 kcal/mol more stable dihydrogen complex **7**. The intramolecular H₂ cleavage in **7** for the regeneration of **1** with the assistance of a S1 atom in the SCS ligand had a free energy barrier of 20.8 kcal/mol (**7** → **TS_{7,1}**). We also examined the stability of an isomer of **4** with a proton on S2, which could be formed by transferring the hydroxyl proton nearby the Ni in **5** to S2 through **TS_{5,6}** with a free energy barrier of 29.3 kcal/mol, and found **6** was 9.1 less stable than **4**. The relative energies in Figure 2 show **4** and **TS_{1,2}** were the rate-determining states in Cycle 1 with a total free energy barrier of 23.2 kcal/mol (**4** → **TS_{1,2}**), which indicates the reaction could easily happen at room temperature for a quick formation of formic acid.

2.2. Influence of Substituents in the SCS Ligand

To understand the influence of various functional groups in the SCS pincer ligand to the catalytic activity and find out potential nickel complexes with better catalytic performance, we built ten SCS nickel complexes (**1a–1j**, Figure 4) by replacing the amino hydrogens (R) and the methyl group in the pyridinium ring (R') in **1** with various substituents. Considering the difficulties in synthesizing asymmetric SCS pincer ligand, we also proposed five complexes with symmetrical amine groups in the SCS pincer ligand (**1'k–1'o**, Figure 4). Similar nickel complexes with symmetrical amine groups in SCS ligand were recently reported by Hu and co-workers [43]. Since the free energy profile in Figure 2 indicates that **4** and **TS**_{1,2} were the rate-determining states in Cycle 1, and **TS**_{7,1} was very close to **TS**_{1,2} in relative energy, we calculated the relative free energies of **4** → **TS**_{1,2} and **4** → **TS**_{7,1} with different functional groups (Table 1).

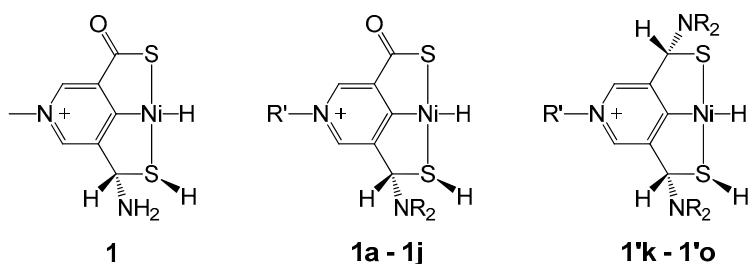


Figure 4. Proposed SCS nickel pincer complexes with different substituents at R and R'.

Table 1. Relative free energies of **4** → **TS**_{1,2} and **4** → **TS**_{7,1} with different functional groups at R and R' in the SCS nickel pincer complexes.

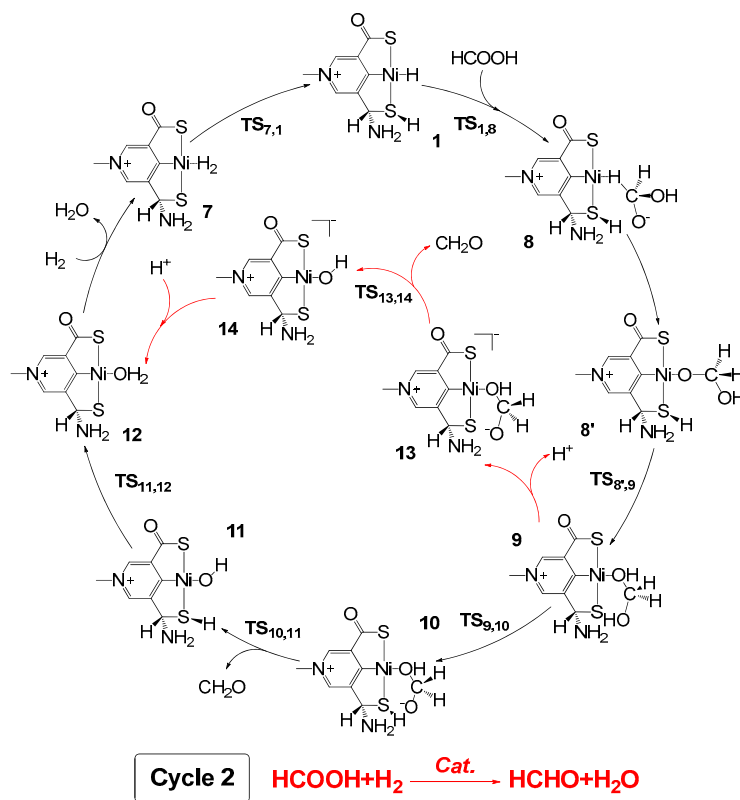
	R	R'	4 → TS _{1,2}	4 → TS _{7,1}
	(kcal/mol)			
1	H	CH ₃	23.2	23.0
1a	F	CH ₃	23.9	23.7
1b	Cl	CH ₃	22.9	22.5
1c	Br	CH ₃	22.2	21.3
1d	CH ₃	CH ₃	22.6	23.0
1e	H	H	23.6	23.5
1f	H	COOH	23.4	21.0
1g	H	NH ₂	22.9	23.3
1h	H	F	23.3	22.5
1i	H	Cl	23.3	20.9
1j	H	CN	23.2	22.0
1'k	H	CH ₃	24.6	25.2
1'l	F	CH ₃	25.3	24.5
1'm	Cl	CH ₃	22.9	22.2
1'n	Br	CH ₃	22.5	20.8
1'o	CH ₃	CH ₃	24.4	25.5

Comparing the calculated relative free energies listed in Table 1, we can see complex **1c** with R = Br and R' = CH₃ had the lowest total free energy barrier of 22.2 kcal/mol, while **1'o** had the highest

barrier of 25.5 kcal/mol. Such a 3.3 kcal/mol difference in free energy barriers indicates that the substituents at R and R' in the SCS ligand have moderate influences on catalytic activity because those functional groups are far away from the reaction center and have limited contributions to the electron density on nickel.

2.3. Hydrogenation of Formic Acid to Formaldehyde and Water

The relative free energies listed in Table 1 indicate **1** and its derivatives were promising candidates for catalytic hydrogenation of CO₂ to formic acid under mild conditions. We further investigated the catalytic activity of **1** for hydrogenation of formic acid. Scheme 2 and Figure 5 are a predicted mechanism for the hydrogenation of HCOOH to CH₂O and H₂O catalyzed by **1** (Cycle 2), and the corresponding reaction coordinate with relative free energies. The optimized structures of stable intermediates, **8'** and **12**, and transition states for hydride transfer (TS_{1,8}), proton transfers (TS_{9,10} and TS_{11,12}), and C–O bond cleavages (TS_{10,11} and TS_{13,14}) are displayed in Figure 6.



Scheme 2. Predicted mechanism for the hydrogenation of formic acid to formaldehyde and water catalyzed by **1** (Cycle 2). The deprotonation pathway is shown with red arrows.

When a formic acid molecule approaches **1**, it can take the hydride on Ni and forms an anionic group HOCH₂O[−] through an 18.5 kcal/mol barrier transition state TS_{1,8}. HOCH₂O[−] in **8** could easily reorient and form an 18.4 kcal/mol more stable isomer **8'** with a strong Ni–O bond (1.893 Å). Then the proton on S1 transferred to the oxygen atom bonding to Ni and formed a methanediol molecule through TS_{8,9}. After the formation of methanediol in **9**, there are two possible ways for the formation of formaldehyde, intramolecular proton transfer, and deprotonation to solvent. In the intramolecular proton transfer pathway, the hydroxyl proton far away from Ni transfers to S1 and forms intermediate **10**. Then a CH₂O molecule can easily be released with C–O bond cleavage through TS_{10,11}, which was only 0.8 kcal/mol higher than **10**. The hydroxyl group left on Ni then takes the proton on S1 and forms a water molecule in intermediate **12**. Instead of intramolecular proton transfer, the hydroxyl proton far away from Ni could be deprotonated in the solvent and form an anionic intermediate **13** with a free energy barrier of 31.5 kcal/mol. The following transition state

(TS_{13,14}) for the release of formaldehyde with a C–O bond cleavage was only 1.7 kcal/mol higher than **13**. The hydroxyl anion in **14** can easily recapture a proton in the solvent and form a water molecule. The H₂O/H₂ exchange in **12** for the formation of **7** was an only 2.9 kcal/mol uphill step.

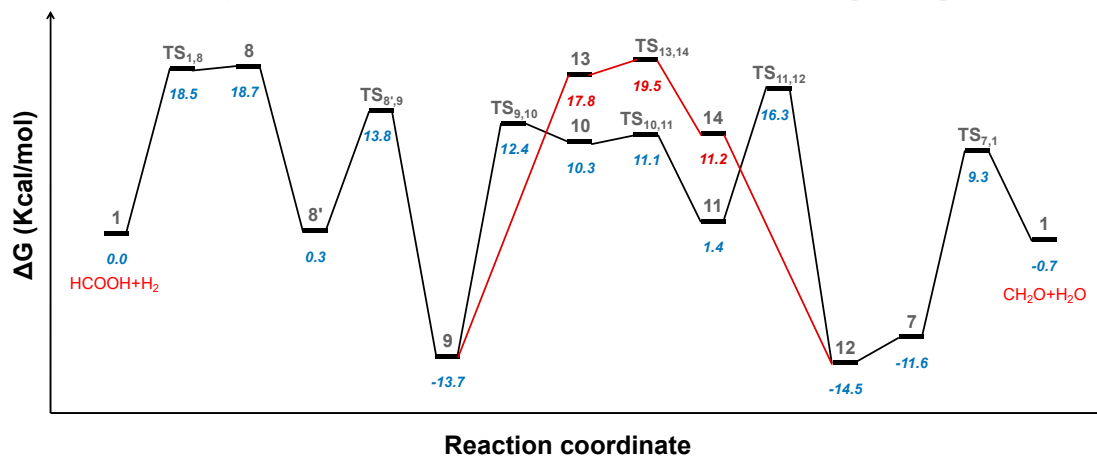


Figure 5. Free energy profile for the hydrogenation of formic acid to formaldehyde and water catalyzed by **1** (Cycle 2). Solvent corrected relative free energies are shown in italic. The deprotonation pathway is shown in red.

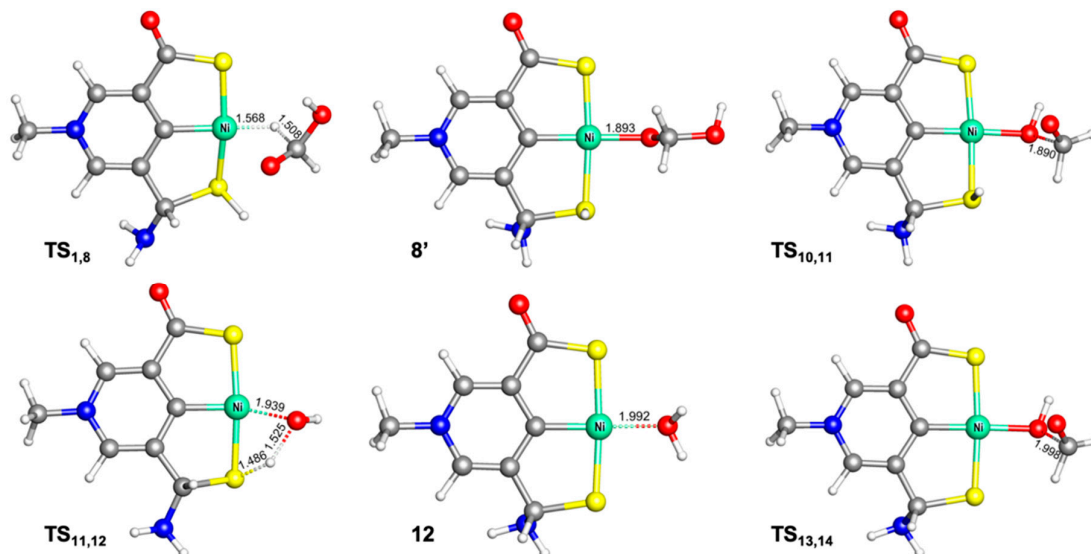


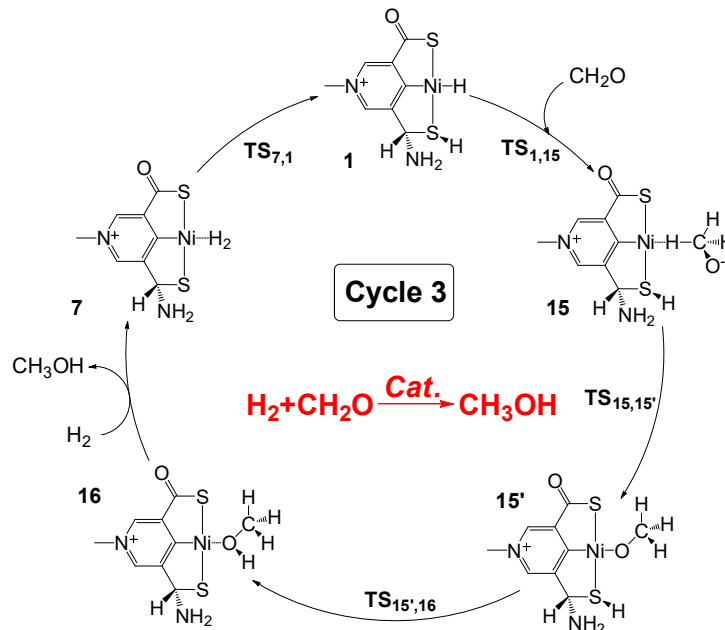
Figure 6. Optimized structures of TS_{1,8} (508.7i cm⁻¹), 8', TS_{10,11} (262.4i cm⁻¹), TS_{11,12} (1352.3i cm⁻¹), **12**, and TS_{13,14} (189.9i cm⁻¹). Bond lengths are in Å.

It is worth noting that the relative free energies of **13** and TS_{13,14} were calculated based on an experimental value of -262.5 kcal/mol for the solvent-free energy of the proton in water [44]. The solvent environment will strongly influence the free energy barriers of this reaction pathway and may lead to a lower total free energy barrier or even a different mechanism for hydrogenation of CO₂ and formic acid [45].

2.4. Hydrogenation of Formaldehyde to Methanol

Scheme 3 is the mechanism for the hydrogenation of formaldehyde to methanol (Cycle 3). The corresponding free energy profile and optimized key structures in Cycle 3 are displayed in Figures 7 and 8, respectively. When a formaldehyde molecule approaches **1**, the hydride on Ni can easily be

transferred to its carbon atom for the formation of a methoxy anion through transition state $TS_{1,15}$ (Figure 8), which was only 7.3 kcal/mol higher than **1** in free energy. The rotation of methoxy anion in **15** formed a 22.5 kcal/mol more stable isomer **15'** with a strong Ni–O bond (1.881 Å). Then a methanol molecule was formed with the transfer of the proton on S1 to the oxygen in methoxy through $TS_{15,16}$. The CH_3OH/H_2 exchange in **16** for the regeneration of **7** was a 6.0 kcal/mol uphill step. The total free energy barrier of Cycle 3 was 25.8 kcal/mol ($16 \rightarrow TS_{7,1}$).



Scheme 3. Predicted mechanism for hydrogenation of formaldehyde.

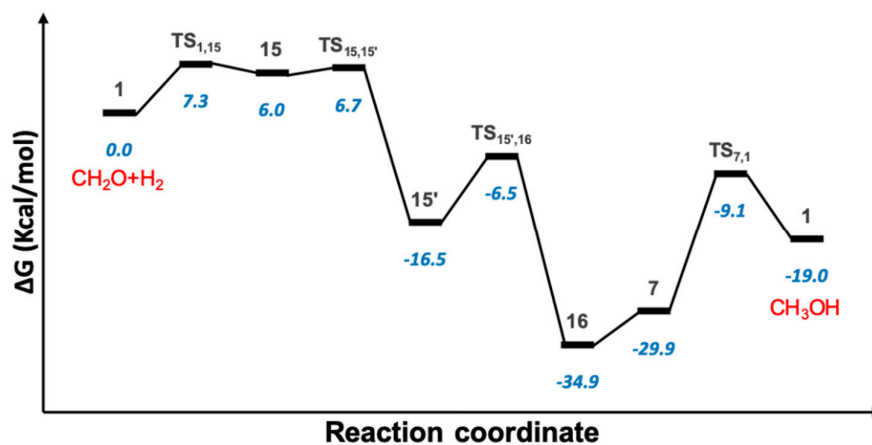


Figure 7. Free energy profile for the hydrogenation of formaldehyde to methanol catalyzed by **1** (Cycle 3). Solvent corrected relative free energies are shown in italic.

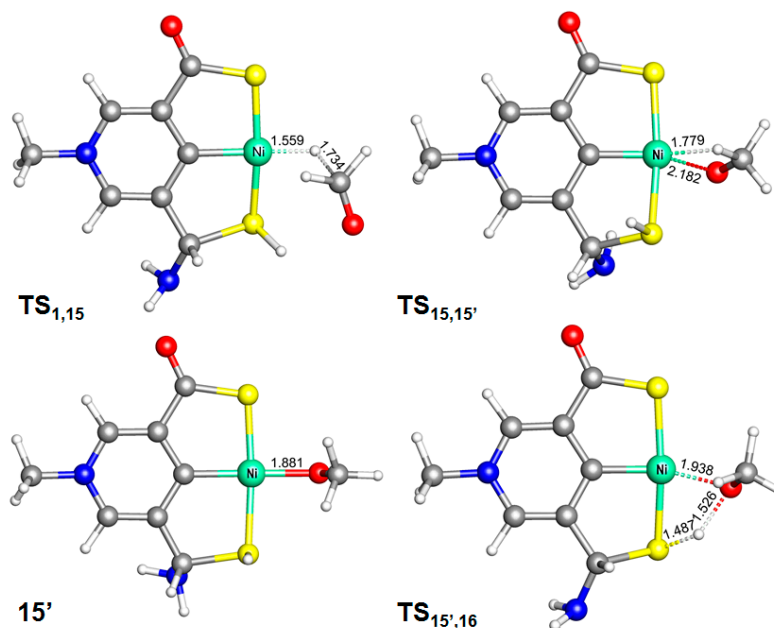


Figure 8. Optimized structures of $15'$, $TS_{1,15}$ ($532.2i\text{ cm}^{-1}$), $TS_{15,15'}$ ($191.8i\text{ cm}^{-1}$), and $TS_{15',16}$ ($1347.0i\text{ cm}^{-1}$). Bond lengths are in Å.

3. Computational Details

Gaussian 09 suite of programs (Revision E.01, Gaussian, Inc., Wallingford, CT, USA, 2009) [46] were used for all DFT calculations with the M06 functional [47]. The all-electron 6-31++G(d,p) basis set [48–50] was used for H, C, N, O, and S atoms, while the Stuttgart relativistic effective core potential basis set (ECP10MDF) was used for Ni [51]. Numerical integrations were at the ultrafine grid level (99, 590). The reliability of M06 functional for this Ni catalytic system was evaluated by comparing the relative free energies between rate-determining states **4** and $TS_{1,2}$ using different density functionals, which are listed in Table S1. The ground states of key intermediates were confirmed as singlets through comparison with their optimized high-spin analogs (Table S2). All structures were fully optimized with the solvent effect corrections using the integral equation formalism polarizable continuum model (IEFPCM) [52] and the solvation model based on density (SMD) radii [53] for water, which could be an environmentally benign, low-cost, and universal solvent for future experimental study. For thermal corrections on optimized structures, 298.15 K temperature, 1 atm pressure, and harmonic potential approximation were used. The experimental value of -262.5 kcal/mol for the free energy of the proton in water [44] was used to calculate deprotonation free energies. Intermediates and transition states were validated through the number of imaginary vibrational modes shown in frequency calculation results. Intrinsic reaction coordinate (IRC) calculations confirmed all transition states were connecting proper reactants and products. The JIMP2 molecular visualizing and manipulating program (version 0.091, Texas A&M University, College Station, TX, USA, 2006) [54] was used to draw 3D molecular structure figures displayed in the text.

4. Conclusions

In summary, our computational study predicted a series of (SCS)Ni(II) pincer complexes as promising candidates for catalytic hydrogenation of CO_2 to formic acid with free energy barriers in a range of 22.2–25.5 kcal/mol in an aqueous solvent. Our DFT calculations reveal a metal–ligand cooperative mechanism with the participation of a sulfur atom in the SCS pincer ligand for the heterolytic cleavage of H_2 . In general, the complexes with electron-donating groups have lower barriers for CO_2 reduction. The free energy barrier differences for the formation of formic acid

catalyzed by proposed nickel complexes with various functional groups at R and R' positions were less than 3.3 kcal/mol, which indicates a moderate substituent effect for the catalytic activities. The above findings not only provide well-defined prototypical base metal complexes as promising candidates for catalytic hydrogenation of CO₂ to formic acid but also point to a way to design efficient catalysts for hydrogenation and dehydrogenation reaction, in which the ligand sulfide group may play an essential role for H₂ activation or formation through MLC.

Our further investigation of the catalytic activities of model complex **1** for hydrogenation of formic acid obtained a free energy barrier of 32.5 kcal/mol (**12** → **8**) for the formation of formaldehyde. The free energy barrier for hydrogenation of formaldehyde to methanol catalyzed by **1** was 25.8 kcal/mol (**16** → **TS_{7,1}**). It is worth noting that although **1** was described as the starting point of the catalytic cycle, it was actually an unstable intermediate in the reaction. The dihydrogen complex **7**, which was a 10.9 kcal/mol more stable isomer of **1**, should be considered as the real catalyst. By comparing all relative free energies in the above three catalytic cycles, we can conclude that the formation of HOCH₂O⁻ anion groups via hydride transfer from Ni to formic acid is the rate-determining step in the whole catalytic hydrogenation of CO₂ to methanol reaction with a total free energy barrier of 34.6 kcal/mol (**16** → **8**). Although such a barrier is slightly too high for a reaction under mild conditions, it is a good starting point for further design of SCS nickel pincer complexes with improved catalytic activities for CO₂ reduction and various (de)hydrogenation reactions.

Moreover, it is worth noting that the pH value of the solvent could impact the catalytic activities and the stability of proposed SCS nickel pincer complexes. Some CO₂ will form hydrogen carbonate in water and make the solvent slightly acidic with the equilibria among dissolved CO₂ gas, carbonic acid, and hydrogen carbonate. In a weak acidic environment, the solvent free energy of proton is slightly higher, which will lead to higher barriers for the deprotonation pathways in Cycle 1 and 2, and make the proposed Ni complexes less likely to be deprotonated, but will not strongly impact the overall barriers of the catalytic cycles.

Supplementary Materials: The following are available online at www.mdpi.com/xxx/s1, Table S1: Absolute and relative free energies of rate-determining states **4** and **TS_{1,2}** calculated by using different density functionals, Table S2: Absolute and relative electronic energies of singlet and triplet states.

Author Contributions: Conceptualization, X.L. and X.Y.; Methodology, X.L. and B.Q.; Writing – original draft, X.L.; Writing—review and editing, B.Q. and X.Y. All authors have read and agreed to the published version of the manuscript.

Funding: This work was supported by the National Natural Science Foundation of China (21673250, 21703256, and 21873107).

Conflicts of Interest: The authors declare no conflict of interest.

References

1. Sakakura, T.; Choi, J.C.; Yasuda, H. Transformation of Carbon Dioxide. *Chem. Rev.* **2007**, *107*, 2365–2387.
2. Cokoja, M.; Bruckmeier, C.; Rieger, B.; Herrmann, W.A.; Kuhn, F.E. Transformation of Carbon Dioxide with Homogeneous Transition-Metal Catalysts: A Molecular Solution to a Global Challenge? *Angew. Chem., Int. Ed. Engl.* **2011**, *50*, 8510–8537.
3. Eby, M.; Zickfeld, K.; Montenegro, A.; Archer, D.; Meissner, K.J.; Weaver, A.J. Lifetime of Anthropogenic Climate Change: Millennial Time Scales of Potential CO₂ and Surface Temperature Perturbations. *J. Climate.* **2009**, *22*, 2501–2511.
4. Aresta, M. *Carbon Dioxide as a Chemical Feedstock*; Wiley-VCH: Weinheim, Germany, 2010.
5. He, M.; Sun, Y.; Han, B. Green Carbon Science: Scientific Basis for Integrating Carbon Resource Processing, Utilization, and Recycling. *Angew. Chem. Int. Ed.* **2013**, *52*, 9620–9633.
6. Jessop, P.G.; Ikariya, T.; Noyori, R. Homogeneous Hydrogenation of Carbon Dioxide. *Chem. Rev.* **1995**, *95*, 259–272.
7. Olah, G.A. Beyond Oil and Gas: The Methanol Economy. *Angew. Chem. Int. Ed.* **2005**, *44*, 2636–2639.
8. Olah, G.A. The Methanol Economy. *Chem. Eng. News.* **2003**, *81*, 5.

9. Olah, G.A.; Goepfert, A.; Prakash, G.K. Surya. Chemical Recycling of Carbon Dioxide to Methanol and Dimethyl Ether: From Greenhouse Gas to Renewable, Environmentally Carbon Neutral Fuels and Synthetic Hydrocarbons. *J. Org. Chem.* **2009**, *74*, 487–498.
10. Nielsen, M.; Alberico, E.; Baumann, W.; Drexler, H.J.; Junge, H.; Gladiali, S.; Beller, M. Low-Temperature Aqueous-Phase Methanol Dehydrogenation to Hydrogen and Carbon Dioxide. *Nature.* **2013**, *495*, 85–89.
11. Natte, K.; Neumann, H.; Beller, M.; Jagadeesh, R.V. Transition-Metal-Catalyzed Utilization of Methanol as a C1 Source in Organic Synthesis. *Angew. Chem. Int. Ed.* **2017**, *56*, 6384–6394.
12. Rodríguez-Lugo, R.E.; Trincado, M.; Vogt, M.; Tewes, F.; Santiso-Quinones, G.; Grützmacher, H. A Homogeneous Transition Metal Complex for Clean Hydrogen Production from Methanol-Water Mixtures. *Nat. Chem.* **2013**, *5*, 342–347.
13. Onishi, N.; Laurenczy, G.; Beller, M.; Himeda, Y. Recent Progress for Reversible Homogeneous Catalytic Hydrogen Storage in Formic Acid and in Methanol. *Coordin. Chem. Rev.* **2018**, *373*, 317–332.
14. Goepfert, A.; Czaun, M.; Jones, J.P.; Prakash, G.K.S.; Olah, G.A. Recycling of Carbon Dioxide to Methanol and Derived Products-Closing the Loop. *Chem. Soc. Rev.* **2014**, *43*, 7995–8048.
15. Bernskoetter, W.H.; Hazari, N. Reversible Hydrogenation of Carbon Dioxide to Formic Acid and Methanol: Lewis Acid Enhancement of Base Metal Catalysts. *Acc. Chem. Res.* **2017**, *50*, 1049–1058.
16. Ribeiro, A.P.C.; Martins, L.M.D.R.S.; Pombeiro, A.J.L. Carbon Dioxide-to-Methanol Single-Pot Conversion using a C-scorpionate Iron (II) Catalyst. *Green Chem.* **2017**, *19*, 4811–4815.
17. Lane, E.M.; Zhang Y.; Hazari, N.; Bernskoetter, W.H. Sequential Hydrogenation of CO₂ to Methanol Using a Pincer Iron Catalyst. *Organometallics*, **2019**, *38*, 15, 3084–3091.
18. Schneidewind, J.; Adam, R.; Baumann, W.; Jackstell, R.; Beller, M. Low-Temperature Hydrogenation of Carbon Dioxide to Methanol with a Homogeneous Cobalt Catalyst. *Angew. Chem., Int. Ed.* **2017**, *56*, 1890–1893.
19. Kar, S.; Goppert, A.; Kothandaraman, J.; Prakash, G.K.S. Manganese-Catalyzed Sequential Hydrogenation of CO₂ to Methanol via Formamide. *ACS Catal.* **2017**, *7*, 9, 6347–6351.
20. Artz, J.; Müller, T.E.; Thenert, K.; Kleinekorte, J.; Meys, R.; Sternberg, A.; Bardow, A.; Leitner, W. Sustainable Conversion of Carbon Dioxide: An Integrated Review of Catalysis and Life Cycle Assessment. *Chem. Rev.* **2018**, *118*, 434–504.
21. Kar, S.; Kothandaraman, J.; Goepfert, A.; Surya Prakash, G.K. Advances in Catalytic Homogeneous Hydrogenation of Carbon Dioxide to Methanol. *J. CO₂ Util.* **2018**, *23*, 212–218.
22. Schmeier, T.J.; Dobreiner, G.E.; Crabtree, R.H.; Hazari, N. Secondary Coordination Sphere Interactions Facilitate the Insertion Step in an Iridium (III) CO₂ Reduction Catalyst. *J. Am. Chem. Soc.* **2011**, *133*, 9274–9277.
23. Tominaga, K.; Sasaki, Y.; Watanabe, T.; Saito, M. Homogeneous Hydrogenation of Carbon Dioxide to Methanol Catalyzed by Ruthenium Cluster Anions in the Presence of Halide Anions. *Bull. Chem. Soc. Jpn.* **1995**, *68*, 2837–2842.
24. Kar, S.; Sen, R.; Goepfert, A.; Prakash, G.K.S. Integrative CO₂ Capture and Hydrogenation to Methanol with Reusable Catalyst and Amine: Toward a Carbon Neutral Methanol Economy. *J. Am. Chem. Soc.* **2018**, *140*, 1580–1583.
25. Huff, C.A.; Sanford, M.S. Cascade Catalysis for the Homogeneous Hydrogenation of CO₂ to Methanol. *J. Am. Chem. Soc.* **2011**, *133*, 18122–18125.
26. Rezayee, N.M.; Huff, C.A.; Sanford, M.S. Tandem Amine and Ruthenium Catalyzed Hydrogenation of CO₂ to Methanol. *J. Am. Chem. Soc.* **2015**, *137*, 1028–1031.
27. Tominaga, K.-I.; Sasaki, Y.; Kawai, M.; Watanabe, T.; Saito, M. Ruthenium Complex Catalysed Hydrogenation of Carbon Dioxide to Carbon Monoxide, Methanol and Methane. *J. Chem. Soc. Chem. Commun.* **1993**, 629–631.
28. Kothandaraman, J.; Goepfert, A.; Czaun, M.; Olah, G.A.; Prakash, G.K.S. Conversion of CO₂ from Air into Methanol Using a Polyamine and a Homogeneous Ruthenium Catalyst. *J. Am. Chem. Soc.* **2016**, *138*, 778–781.
29. Wesselbaum, S.; Moha, V.; Meuresch, M.; Brosinski, S.; Thenert, K.M.; Kothe, J.; vom Stein, T.; Englert, U.; Holscher, M.; Klankermayer, J.; Leitner, W. Hydrogenation of Carbon Dioxide to Methanol using a Homogeneous Ruthenium-Triphos Catalyst: from Mechanistic Investigations to Multiphase Catalysis. *Chem. Sci.* **2015**, *6*, 693–704.

30. Wesselbaum, S.; vom Stein, T.; Klankermayer, J.; Leitner, W. Hydrogenation of Carbon Dioxide to Methanol by Using a Homogeneous Ruthenium Phosphine Catalyst. *Angew. Chem. Int. Ed.* **2012**, *51*, 7499–7502.
31. Kar, S.; Sen, R.; Kothandaraman, J.; Goeppert, A.; Chowdhury, R.; Munoz, S.B.; Haiges, R.; Prakash, G.K.S. Mechanistic Insights into Ruthenium-Pincer-Catalyzed Amine-Assisted Homogeneous Hydrogenation of CO₂ to Methanol. *J. Am. Chem. Soc.* **2019**, *141*, 7, 3160–3170.
32. Tsurusaki, A.; Murata, K.; Onishi, N.; Sordakis, K.; Laurency, G.; Himeda, Y. Investigation of Hydrogenation of Formic Acid to Methanol using H₂ or Formic Acid as a Hydrogen Source. *ACS Catal.* **2017**, *7*, 1123–1131.
33. Wang, W.; Qiu, B.; Yang, X. Computational Prediction of Pentadentate Iron and Cobalt Complexes as a Mimic of Mono-iron Hydrogenase for the Hydrogenation of Carbon Dioxide to Methanol. *Dalton Trans.* **2019**, *48*, 8034–8038.
34. Yan, X.; Ge, H.; Yang, X. Hydrogenation of CO₂ to Methanol Catalyzed by Cp*Co Complexes: Mechanistic Insights and Ligand Design. *Inorg. Chem.* **2019**, *58*, 5494–5502.
35. Ge, H.; Chen, X.; Yang, X. Hydrogenation of carbon dioxide to methanol catalyzed by iron, cobalt, and manganese cyclopentadienone complexes: Mechanistic insights and computational design. *Chem. Eur. J.* **2017**, *23*, 8850–8856.
36. Chen, X.; Ge, H.; Yang, X. Newly designed manganese and cobalt complexes with pendant amines for the hydrogenation of CO₂ to methanol: A DFT study. *Catal. Sci. Technol.* **2017**, *7*, 348–355.
37. Chen, X.; Yang, X. Bioinspired Design and Computational Prediction of Iron Complexes with Pendant Amines for the Production of Methanol from CO₂ and H₂. *J. Phys. Chem. Lett.* **2016**, *7*, 1035–1041.
38. Desguin, B.; Zhang, T.; Soumillion, P.; Hols, P.; Hu, J.; Hausinger, R.P. A Tethered Niacin-Derived Pincer Complex with a Nickel-Carbon Bond in Lactate Racemase. *Science* **2015**, *349*, 66–69.
39. Qiu, B.; Yang, X. A Bio-inspired Design and Computational Prediction of Scorpion-Like SCS Nickel Pincer Complexes for Lactate Racemization. *Chem. Commun.* **2017**, *53*, 11410–11413.
40. Qiu, B.; Wang, W.; Yang, X. Computational Prediction of Ammonia-Borane Dehydrocoupling and Transfer Hydrogenation of Ketones and Imines Catalyzed by SCS Nickel Pincer Complexes. *Front. Chem.* **2019**, *7*, 627.
41. Yang, X.; Hall, M.B. Monoiron Hydrogenase Catalysis: Hydrogen Activation with the Formation of a Dihydrogen, Fe–H^{δ-}...H^{δ+}–O, Bond and Methenyl-H₄MPT⁺ Triggered Hydride Transfer. *J. Am. Chem. Soc.* **2009**, *131*, 10901–10908.
42. Shi, R.; Wodrich, M.D.; Pan, H.; Tirani, F.F.; Hu, X. Functional Models of the Nickel Pincer Nucleotide Cofactor of Lactate Racemase. *Angew. Chem. Int. Ed.* **2019**, *58*, 16869–16872.
43. Xu, T.; Wodrich, M.D.; Scopelliti, R.; Corminboeuf, C.; Hu, X. Nickel Pincer Model of the Active Site of Lactate Racemase Involves Ligand Participation in Hydride Transfer. *Proc. Natl. Acad. Sci. USA* **2017**, *114*, 1242–1245.
44. Topol, I.A.; Tawa, G.J.; Burt, S.K.; Rashin, A.A. Calculation of Absolute and Relative Acidities of Substituted Imidazoles in Aqueous Solvent. *J. Phys. Chem. A.* **1997**, *101*, 10075–10081.
45. Wiedner, E.S.; Linehan, J.C. Making a Splash in Homogeneous CO₂ Hydrogenation: Elucidating the Impact of Solvent on Catalytic Mechanisms. *Chem. Eur. J.* **2018**, *24*, 16964–16971.
46. Frisch, M.J.; Trucks, G.W.; Schlegel, H.B.; Scuseria, G.E.; Robb, M.A.; Cheeseman, J.R.; Scalmani, G.; Barone, V.; Mennucci, B.; Petersson, G.A.; Nakatsuji, H.; Caricato, M.; Li, X.; Hratchian, H.P.; Izmaylov, A.F.; Bloino, J.; Zheng, G.; Sonnenberg, J.L.; Hada, M.; Ehara, M.; Toyota, K.; Fukuda, R.; Hasegawa, J.; Ishida, M.; Nakajima, T.; Honda, Y.; Kitao, O.; Nakai, H.; Vreven, T.; Montgomery, J.A., Jr.; Peralta, J.E.; Ogliaro, F.; Bearpark, M.; Heyd, J.J.; Brothers, E.; Kudin, K.N.; Staroverov, V.N.; Keith, T.; Kobayashi, R.; Normand, J.; Raghavachari, K.; Rendell, A.; Burant, J.C.; Iyengar, S.S.; Tomasi, J.; Cossi, M.; Rega, N.; Millam, J.M.; Klene, M.; Knox, J.E.; Cross, J.B.; Bakken, V.; Adamo, C.; Jaramillo, J.; Gomperts, R.; Stratmann, R.E.; Yazyev, O.; Austin, A.J.; Cammi, R.; Pomelli, C.; Ochterski, J.W.; Martin, R.L.; Morokuma, K.; Zakrzewski, V.G.; Voth, G.A.; Salvador, P.; Dannenberg, J.J.; Dapprich, S.; Daniels, A.D.; Farkas, O.; Foresman, J.B.; Ortiz, J.V.; Cioslowski, J.; Fox, D.J. Gaussian 09, Revision E.01; Gaussian, Inc.: Wallingford, CT, USA, **2009**.
47. Zhao, Y.; Truhlar, D.G. The M06 Suite of Density Functionals for Main Group Thermochemistry, Thermochemical Kinetics, Noncovalent Interactions, Excited States, and Transition Elements: Two New Functionals and Systematic Testing of Four M06-Class Functionals and 12 Other Functionals. *Theor. Chem. Acc.* **2008**, *120*, 215–241.

48. Krishnan, R.; Binkley, J.S.; Seeger, R.; Pople, J.A. Self-Consistent Molecular Orbital Methods. XX. A Basis Set for Correlated Wave Functions. *J. Chem. Phys.* **1980**, *72*, 650–654.
49. Hariharan, P.C.; Pople, J.A. The Influence of Polarization Functions on Molecular Orbital Hydrogenation Energies. *Theor. Chim. Acta.* **1973**, *28*, 213–222.
50. Hehre, W.J.; Ditchfield, R.; Pople, J.A. Self-Consistent Molecular Orbital Methods. XII. Further Extensions of Gaussian-Type Basis Sets for Use in Molecular Orbital Studies of Organic Molecules. *J. Chem. Phys.* **1972**, *56*, 2257–2261.
51. Martin, J.M.L.; Sundermann, A. Correlation Consistent Valence Basis Sets for Use with the Stuttgart-Dresden-Bonn Relativistic Effective Core Potentials: The Atoms Ga-Kr and In-Xe. *J. Chem. Phys.* **2001**, *114*, 3408–3420.
52. Tomasi, J.; Mennucci, B.; Cammi, R. Quantum Mechanical Continuum Solvation Models. *Chem. Rev.* **2005**, *105*, 2999–3093.
53. Marenich, A.V.; Cramer, C.J.; Truhlar, D.G. Universal Solvation Model Based on Solute Electron Density and on a Continuum Model of the Solvent Defined by the Bulk Dielectric Constant and Atomic Surface Tensions. *J. Phys. Chem. B.* **2009**, *113*, 6378–6396.
54. Manson, J.; Webster, C.E.; Hall, M.B. JIMP2, version 0.091, A Free Program for Visualizing and Manipulating Molecules; Texas A&M University: College Station, TX, USA, **2006**.



© 2020 by the authors. Licensee MDPI, Basel, Switzerland. This article is an open access article distributed under the terms and conditions of the Creative Commons Attribution (CC BY) license (<http://creativecommons.org/licenses/by/4.0/>).